

# Optical properties and UV photoresponse of $\text{Na}_{2x}\text{Zn}_{1-x}\text{O}$ thin film

Jianguo Lv<sup>1</sup> · Wenhao Wang<sup>1</sup> · Min Zhao<sup>1</sup> · Yuebing Cheng<sup>1</sup> · Weili Zhu<sup>1</sup> ·  
Gang He<sup>2</sup> · Miao Zhang<sup>2</sup> · Zhaoqi Sun<sup>2</sup> · Xiaoshuang Chen<sup>3</sup>

Received: 18 July 2016 / Accepted: 22 August 2016 / Published online: 25 August 2016  
© Springer Science+Business Media New York 2016

**Abstract**  $\text{Na}_{2x}\text{Zn}_{1-x}\text{O}$  thin films were successfully synthesized on quartz glass substrates by sol–gel method. The effect of Na content on the microstructure, optical properties and UV photoresponse of the thin films was investigated using X-ray diffraction, optical absorbance, photoluminescence, and conductivity measurements. The results indicate that the  $\text{Na}_{0.04}\text{Zn}_{0.98}\text{O}$  thin film exhibits the strongest preferential *c*-axis orientation with a polycrystalline hexagonal wurtzite structure and has the largest optical band gap. An obvious decrease in crystal size has been observed with the increasing of Na content. A weak ultraviolet emission band at about 381 nm and a strong visible emission band have been observed in the photoluminescence spectra. The  $\text{Na}_{0.04}\text{Zn}_{0.98}\text{O}$  thin film has the shortest growth and decay time (45 and 18 s, respectively) and the largest photoresponse. The results indicate that the photoresponse can be effectively improved by means of moderate Na doping.

## 1 Introduction

Due to the wide direct band gap (3.37 eV) and large exciton binding energy (60 meV at 300 K), zinc oxide (ZnO) has been widely applied in ultraviolet (UV) light emitting diodes [1], UV photodetectors [2], piezoelectric devices [3], solar cells [4] and phototransistors [5] etc. However, the photodetector based on pure ZnO suffers from the weak responsivity drawbacks. It is well known that the photoconduction in the ZnO is controlled by oxygen adsorption and desorption on the surface of ZnO [6, 7]. Photosensitivity and photoresponse of ZnO strongly depend on the surface condition, crystal structure and doping. Some efforts have been made to obtain ZnO with fast, sensitive, and high UV response by passivating the surface of ZnO [8, 9], modifying the nanostructure [10, 11] or appropriately doping [12, 13]. Dhara and Giri [9] reported that UV photosensitivity and photoresponse of the vertically aligned ZnO nanowires can be improved by means of rapid thermal annealing. Porter et al. [12] thought that the photoconductive response could be significantly improved by varying the relative doping concentrations of nitrogen and tellurium. Therefore, surface modification, structural improvement and doping can improve the photosensitivity and photoresponse of ZnO. However, the preparation of ZnO doped with Na by a facile and low-cost method and the study of photoconductive UV detector based on the Na doped ZnO thin film are seldom.

In this letter, the effects of Na doping on the microstructure and optical properties of  $\text{Na}_{2x}\text{Zn}_{1-x}\text{O}$  thin films have been described in detail. The enhanced photoconduction and photoresponse behavior by Na doping have been observed. The formation mechanism of the photoresponse behavior has been explained based on the experimental results.

✉ Min Zhao  
zhaomin@hftc.edu.cn

✉ Gang He  
hegang@ahu.edu.cn

✉ Zhaoqi Sun  
szq@ahu.edu.cn

<sup>1</sup> School of Electronic and Information Engineering, Hefei Normal University, Hefei 230601, China

<sup>2</sup> School of Physics and Material Science, Anhui University, Hefei 230039, China

<sup>3</sup> National Laboratory for Infrared Physics, Shanghai Institute of Technical Physics, Chinese Academy of Sciences, Shanghai 200083, China

## 2 Experimental

Undoped and Na doped ZnO thin films were prepared by sol–gel method. All chemicals were of analytical grade and used as purchased without further purification. Zinc acetate dehydrate [Zn(CH<sub>3</sub>COO)<sub>2</sub>·2H<sub>2</sub>O], sodium chloride [NaCl] and monoethanol amine (MEA) [HO(CH<sub>2</sub>)<sub>2</sub>NH<sub>2</sub>] were used as precursors. The appropriate amounts of zinc acetate dehydrate, sodium chloride and monoethanol amine was dissolved into 80 mL of ethylene glycol monomethyl ether [CH<sub>3</sub>OCH<sub>2</sub>CH<sub>2</sub>OH] at room temperature. The total amount of metal (Zn and Na) was fixed at 0.5 mol/L and the molar ratio of monoethanol amine to metal ions was kept at 1:1. The obtained solution was magnetically stirred at 60 °C for 2 h to get a homogeneous sol, which served as the coating sol after being kept for 24 h. Quartz glass substrates (15 mm × 15 mm) were cleaned ultrasonically in acetone and deionized water, and dried in an oven. The quartz substrate was spin coated with sol and heated at 150 °C for 10 min. This above process was repeated for ten times to obtain the desired thickness. After that, the thin film was annealed in a tube furnace at 800 °C for 4 h in air.

Microstructure of the thin films were examined using a X-ray diffractometry (XRD, TD-3500) with Cu Kα radiation (λ = 0.15418 nm) operating at 40 kV and 30 mA. The 2θ scan range was 30°–80° with a step of 0.02°. Optical absorbance spectra were measured using a UV–Vis spectrophotometer (UV–Vis, SHIMADZU UV2550) in the wavelength range of 300–600 nm. Photoluminescence (PL) spectra of the thin films were performed by a laser micro-Raman spectrometer (Renishaw in Via-Reflex) using He–Cd laser as light source excited at 325 nm. Photoresponses of the thin films were measured by an electrochemical workstation (CHI-660D) at a fixed bias of 5 V by switching the UV light (λ = 254 nm) with a power intensity of 14 μW/cm<sup>2</sup>.

## 3 Results and discussion

XRD patterns of ZnO, Na<sub>0.04</sub>Zn<sub>0.98</sub>O and Na<sub>0.16</sub>Zn<sub>0.92</sub>O thin films are shown in Fig. 1. It can be seen that three peaks appear at 2θ = 31.77, 34.42 and 36.26° in the patterns are assigned to (100), (002) and (101) planes of the hexagonal phase ZnO (JCPDS 36-1451). No peaks corresponding to either Na metal or its oxides has been observed in the Na-doped films, which suggested that there is no Na-related phase present within the detection limit. It also can be seen that Na doping has the obvious effect on the crystal orientation of ZnO thin film. In order to characterize quantitatively the crystal orientation of the thin films, the

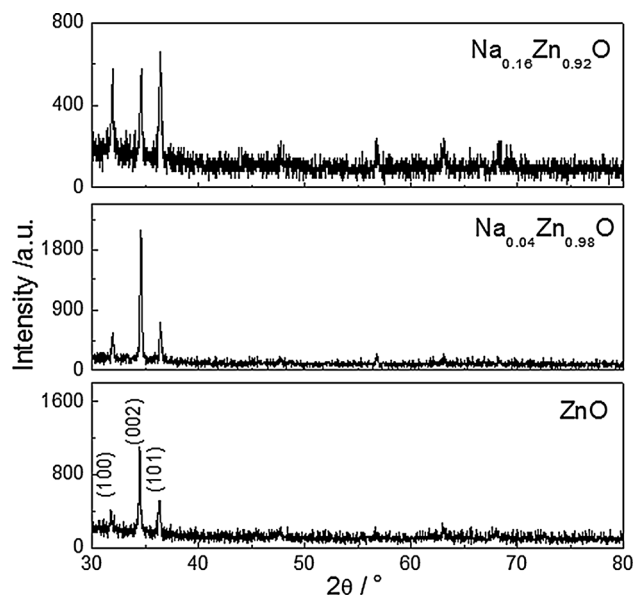


**Fig. 1** XRD patterns of ZnO, Na<sub>0.04</sub>Zn<sub>0.98</sub>O and Na<sub>0.16</sub>Zn<sub>0.92</sub>O thin films

texture coefficient  $TC_{(hkl)}$  can be obtain by applying the following formula [14]:

$$TC_{(hkl)} = \frac{I_{(hkl)}/I_{0(hkl)}}{\frac{1}{N} \sum_N I_{(hkl)}/I_{0(hkl)}} \quad (1)$$

where  $I_{(hkl)}$  is the experimental relative intensity of (hkl) plane,  $I_{0(hkl)}$  is the standard relative intensity of (hkl) plane and  $N$  is the total number of peaks from the thin film. The value,  $TC_{(hkl)} = 1$ , represents the sample with randomly oriented crystallites, while higher value indicates the abundance of crystal orientation along (hkl) direction [14]. In our case,  $N = 3$  because three diffraction peaks come from (100), (002) and (101) planes are involved.  $TC_{(hkl)}$  of ZnO, Na<sub>0.04</sub>Zn<sub>0.98</sub>O and Na<sub>0.16</sub>Zn<sub>0.92</sub>O thin films are listed in Table 1. It can be seen that the  $TC_{(002)}$  of Na<sub>0.04</sub>Zn<sub>0.98</sub>O thin film much larger than 1, which indicated that the sample of Na<sub>0.04</sub>Zn<sub>0.98</sub>O has the best preferential orientation along *c*-axis. Moderate Na doping is in favour of improving preferential *c*-axis orientation of the ZnO. Similar result has been reported by Lai et al. The intensity of the (002) peak increases with increasing Na content to a

**Table 1** Average grain size and texture coefficient of the thin films

Sample	<i>D</i> (nm)	Texture coefficient $TC_{(hkl)}$		
		$TC_{(100)}$	$TC_{(002)}$	$TC_{(101)}$
ZnO	63.7	0.55	2.03	0.42
Na <sub>0.04</sub> Zn <sub>0.98</sub> O	63.5	0.45	2.20	0.35
Na <sub>0.16</sub> Zn <sub>0.92</sub> O	52.2	1.02	1.32	0.66

maximum at  $x = 0.15$ , and it decreases with increasing Na content beyond that point. They thought that suitable Na doping will be helpful in obtaining a preferable  $c$ -orientation of the ZnO film [15]. Average grain size of the thin film is calculated after appropriate background correction by using Scherrer's formula [16]:

$$D = 0.9\lambda/\beta \cos \theta \quad (2)$$

where  $D$  is the grain size,  $\lambda$  is the X-ray wavelength ( $\lambda = 0.15418$  nm),  $\beta$  is the full width at half maximum (FWHM) of the diffraction peak, and  $\theta$  is the diffraction angle. The average grain size of the thin film has been listed in Table 1. It can be seen that the average grain size decreases monotonously with the increasing of Na content. Wang et al. reported that the crystal size of  $\text{Na}_{2x}\text{Zn}_{1-x}\text{O}$  films increases with the increasing of Na content. They considered that the  $\text{Na}_{\text{Zn}}$  defects may increase the  $\text{Zn}_i$  defects, which can promote the growth of ZnO crystal [17]. However, Lin and Tsai [18] thought that the increasing of the Al concentration will enhance the nucleation of the ZnO phase and consequently result in the smaller crystallite size. In our case, the decrease of grain size may be attributed to the increasing nucleation of ZnO as Na content increases.

Figure 2 depicts the UV–Vis absorbance spectra of the undoped ZnO,  $\text{Na}_{0.04}\text{Zn}_{0.98}\text{O}$  and  $\text{Na}_{0.16}\text{Zn}_{0.92}\text{O}$  thin films. The ZnO and  $\text{Na}_{0.16}\text{Zn}_{0.92}\text{O}$  thin films have sharp absorption edge at about 375–385 nm. Compared with undoped ZnO,  $\text{Na}_{0.04}\text{Zn}_{0.98}\text{O}$  exhibits a slight blue-shift of the absorption edge. The optical band gap of the thin film can be calculated by use of the following relationship in the high absorption region [19]:

$$\alpha hv = A(hv - E_g)^n \quad (3)$$

where  $\alpha$  is the absorbance,  $hv$  is the photon energy,  $E_g$  is the optical band gap and  $A$  is a constant. For direct band

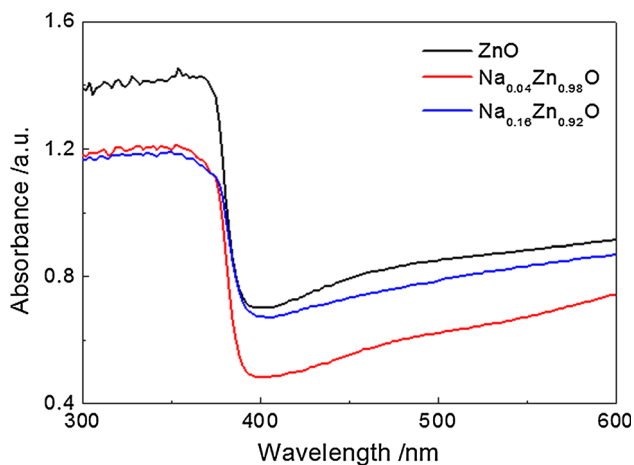


**Fig. 2** Absorbance spectra of  $\text{Na}_{2x}\text{Zn}_{1-x}\text{O}$  thin films

gap semiconductor,  $n = 1/2$ . The functional dependence of  $(\alpha hv)^2$  versus photon energy  $hv$  is shown in Fig. 3. The band gaps of the thin films have been calculated using plots of  $(\alpha hv)^2$  versus  $hv$  and by extrapolating the linear portion of the absorption edge to find the intercept with energy axis. The values of  $E_g$  of the thin films are listed in Table 2. It can be seen that  $E_g$  of ZnO thin film is 3.19 eV. It increases to 3.20 eV when the value of Na doping increases to 0.02. Then  $E_g$  decreases when the value of Na doping increases to 0.08. The shift of the optical absorption edge may be attributed to the changes of the quality of ZnO film [20]. Change of optical band gap energy of ZnO films can also be attributed to the size of micro- and nanostructures present on the surface of the films [21]. Etacheri et al. [22] thought that the increase of optical band gap of Mg doped ZnO can be attributed to the so-called Moss–Burstein effect. Suwanboon et al. [23] considered that the increase of optical band gap might be due to the decrease in the crystallite size of  $\text{Zn}_{1-x}\text{Mg}_x\text{O}$  nanostructures. In our case, the increasing of optical band gap by Na dopants may be attributed to the Na ions, which were incorporated as interstitial donors in the thin film. The decreasing of the optical band gap as the Na dopants increases from 0.02 to 0.08 may be attributed to the change of crystal size and preferential orientation along  $c$ -axis.

Figure 4 shows the room temperature PL spectra of undoped ZnO and Na-doped ZnO thin films. It can be seen that a weak ultraviolet emission centered at about 381 nm and a strong and broad blue–green–yellow (430–640 nm) emission band appeared in the PL spectra. Usually, the UV emission peak originates from the radiative recombination of free excitations corresponding to the near-band edge (NBE) emission of ZnO. The strong green–yellow emission band may be derived from the deep level defects in the ZnO nanostructures. Generally, the blue, green and yellow emission bands are attributed to the deep level defects such

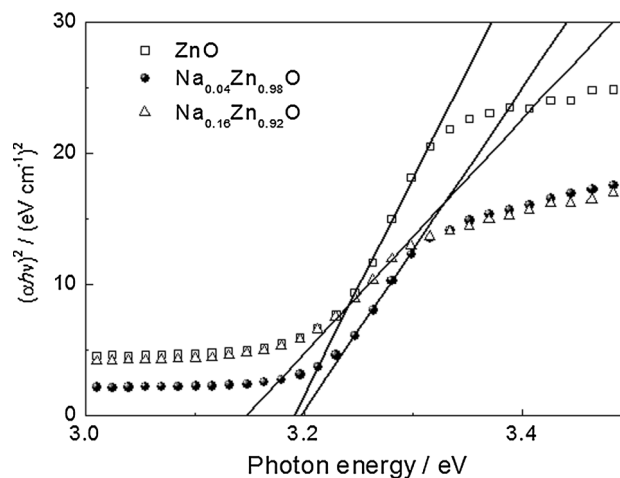


**Fig. 3** Plot of  $(\alpha hv)^2$  versus photon energy for  $\text{Na}_{2x}\text{Zn}_{1-x}\text{O}$  thin films

**Table 2** Optical band gap and photoresponse performance of  $\text{Na}_{2x}\text{Zn}_{1-x}\text{O}$  thin films

Sample	Optical bandgap/eV	$I_{\text{dark}}/\text{nA}$	$I_{\text{p}}/\text{nA}$	Rise time/s	Decay time/s
ZnO	3.19	1.60	16.40	59	26
$\text{Na}_{0.04}\text{Zn}_{0.98}\text{O}$	3.20	19.4	574.8	45	18
$\text{Na}_{0.16}\text{Zn}_{0.92}\text{O}$	3.15	6.83	88.10	57	36

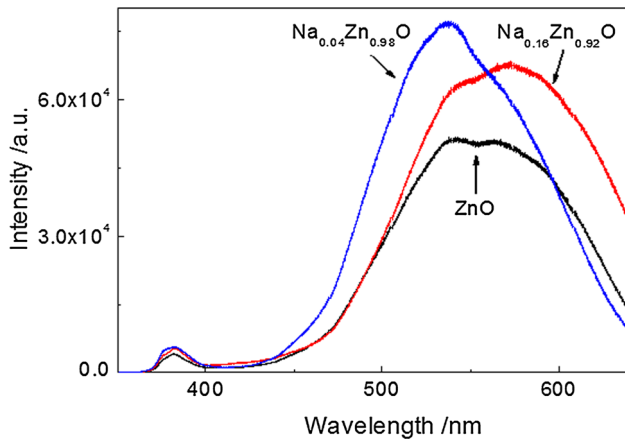


**Fig. 4** PL spectra of  $\text{Na}_{2x}\text{Zn}_{1-x}\text{O}$  thin films

as oxygen vacancies ( $V_{\text{O}}$ ), Zinc vacancies ( $V_{\text{Zn}}$ ), oxygen interstitials ( $\text{O}_i$ ), Zinc interstitials ( $\text{Zn}_i$ ) and oxygen antisites ( $\text{O}_{\text{Zn}}$ ) [24, 25]. The blue emission bands between 450 and 490 nm may be attributed to the electron radiative transition from the deep donor level of  $\text{Zn}_i$  to an acceptor level of  $V_{\text{Zn}}$  [25]. Enhance in blue emission band indicates that deep donor level of  $\text{Zn}_i$  is increased by Na-doping. The green emission at 536 nm is due to the electron radiative transition from the deep donor level of  $\text{Zn}_i$  to an acceptor level caused by singly ionized charged state of the  $V_{\text{Zn}}^-$ . Yang et al. [26, 27] thought that the visible emission band centered at about 570 nm is associated with oxygen vacancies. Kashif et al. [28] considered that the visible emission at 567 nm are associated with the singly ionized oxygen vacancy in ZnO and results from the recombination of a photogenerated hole with the singly ionized charge state of this defect. In our case, the green emission at about 570 nm may be attributed to the point defect of oxygen vacancy in the ZnO. Of all of the samples, the sample of  $\text{Na}_{0.04}\text{Zn}_{0.98}\text{O}$  has the strongest green emission at about 570 nm, indicating the most oxygen vacancies appear in the sample.

To study further the effect of Na doping on the photoresponse (rise and decay), we performed the photoresponse measurement of the thin films under UV light ( $\lambda = 254 \text{ nm}$ ). Figure 5 shows the time dependent photocurrent of the thin films under periodic UV irradiation. Of all the samples, the sample of  $\text{Na}_{0.04}\text{Zn}_{0.98}\text{O}$  has the biggest dark current. The conductance of the thin film increases first and then decreases with the increasing of Na doping.

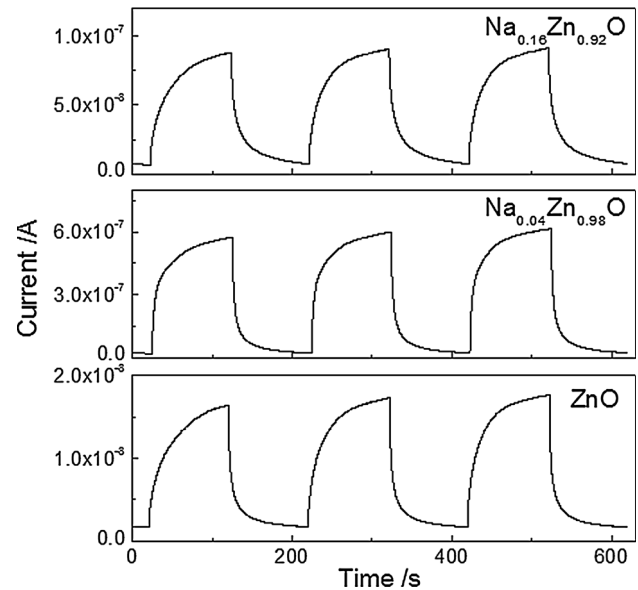


**Fig. 5** Time response of photocurrent under the dark and UV illumination at a fixed bias voltage

As is well known, oxygen vacancy is donor-doping in ZnO thin film [29]. The conductance of the thin film increases with the oxygen vacancy density increase. The result confirm that the number of oxygen vacancies more than others, which is well consistent with the results from the PL spectra. Under the UV irradiation, the photocurrent initially grows very fast and then slowly increased with time and reaches the saturation value. When turn off the UV lamp, the photocurrent take a period of time to recover the initial value. Rise time is defined as the time needed to reach 90 % of the maximum photocurrent value, while the decay time is the time needed to reach 10 % of the maximum photocurrent value. The rise time and decay time of the thin films are listed in Table 2. It is notable that the rise time and decay time of  $\text{Na}_{0.04}\text{Zn}_{0.98}\text{O}$  thin film are 45 s and 18 s, respectively. The result tells us that the performance of the photoconductor can be effectively improved by doping moderate Na. In the absence of UV irradiation, oxygen molecules are adsorbed on the surface by capturing free electrons from the n-type ZnO [ $\text{O}_{2(\text{g})} + e^- \rightarrow \text{O}_{2(\text{ad})}^-$ ], thus creating a low-conductivity depletion layer near the surface [30, 31]. Therefore, the resistance of the thin films should be dominated by the surface barriers. When ZnO thin film is illuminated by UV illumination with photon energies above ZnO band gap, electron–hole pairs are

excited [ $h\nu \rightarrow e^- + h^+$ ]. These electrons/holes easily cross the depletion layers and contribute to the photo conductivity. At the same time, the photogenerated holes can migrate to the surface and neutralize the surface adsorbed oxygen [ $h^+ + O_{2(ad)}^- \rightarrow O_{2(g)}$ ]. The depletion width and the surface potential barrier height gradually reduce until the oxygen desorption and readsorption reach an equilibrium state, which is responsible for the slow rise of photocurrent with a saturation value [9, 31, 32].

## 4 Conclusions

Undoped and Na-doped ZnO thin films were prepared via the sol–gel method on quartz substrates. Microstructure, UV–Vis absorbance spectra, PL spectra and time dependent photocurrent under periodic UV irradiation of the thin films have been measured by X-ray diffractometry, UV–Vis spectrophotometer, laser micro-Raman spectrometer and electrochemical workstation. The effects of Na doping on the microstructure and optical properties of the thin films were investigated systematically. The best preferential orientation along *c*-axis, the largest optical band gap, the most oxygen vacancies, biggest dark current and the shortest rise time and decay time have been observed in the  $Na_{0.04}Zn_{0.98}O$  thin film. These results indicate that the Na doping is an effective method to enhance photoresponse, which is significant for the fabrication of UV photodetectors based on ZnO.

**Acknowledgments** This work was supported by National Natural Science Foundation of China (Nos. 51102072, 51472003, 51272001, 21201052, 51572002), Natural Science Foundation of Anhui Higher Education Institution of China (Nos. KJ2015ZD32, KJ2012Z336, KJ2013A224), Fund for “136” Talent of Hefei Normal University (No. 2014136KJB03), Fund of Hefei Normal University (No. 2015QN05).

## References

1. N.T. Nguyen, S.G. Ri, T. Nagata, K. Ishibashi, K. Takahashi, Y. Tsunekawa, S. Suzuki, T. Chikyow, Epitaxial growth of nonpolar ZnO and n-ZnO/i-ZnO/p-GaN heterostructure on Si(001) for ultraviolet light emitting diodes. *Appl. Phys. Express* **7**, 062102 (2014)
2. J.H. He, Y.H. Lin, M.E. McConney, V.V. Tsukruk, Z.L. Wang, G. Bao, Enhancing UV photoconductivity of ZnO nanobelt by polyacrylonitrile functionalization. *J. Appl. Phys.* **102**, 084303 (2007)
3. Y. Hu, Y. Chang, P. Fei, R.L. Snyder, Z.L. Wang, Designing the electric transport characteristics of ZnO micro/nanowire devices by coupling piezoelectric and photoexcitation effects. *ACS Nano* **4**, 1234–1240 (2010)
4. Q. Zhang, C.S. Dandeneau, X. Zhou, G. Cao, ZnO nanostructures for dye-sensitized solar cells. *Adv. Mater.* **21**, 4087–4108 (2009)
5. W.Y. Weng, S.J. Chang, C.L. Hsu, T.J. Hsueh, A ZnO-nanowire phototransistor prepared on glass substrates. *ACS Appl. Mater. Interfaces* **3**, 162–166 (2011)
6. M. Liu, H.K. Kim, Ultraviolet detection with ultrathin ZnO epitaxial films treated with oxygen plasma. *Appl. Phys. Lett.* **84**, 173–175 (2004)
7. X. Ye, H. Liu, N. Hu, J. Wang, M. Li, Y. Zhang, A novel photoconductive UV detector based on ZnO/RGO composite with enhanced photoresponse performance. *Mater. Lett.* **150**, 126–129 (2015)
8. K. Moazzami, T.E. Murphy, J.D. Phillips, M.C.K. Cheung, A.N. Cartwright, Sub-bandgap photoconductivity in ZnO epilayers and extraction of trap density spectra. *Semicond. Sci. Technol.* **21**, 717 (2006)
9. S. Dhara, P.K. Giri, Enhanced UV photosensitivity from rapid thermal annealed vertically aligned ZnO nanowires. *Nanoscale Res. Lett.* **6**, 504 (2011)
10. X. Wang, M. Liao, Y. Zhong, J.Y. Zheng, W. Tian, T. Zhai, C. Zhi, Y. Ma, J. Yao, Y. Bando, D. Golberg, ZnO hollow spheres with double-yolk egg structure for high-performance photocatalysts and photodetectors. *Adv. Mater.* **24**, 3421–3425 (2012)
11. J.B.K. Law, J.T.L. Thong, Simple fabrication of a ZnO nanowire photodetector with a fast photoresponse time. *Appl. Phys. Lett.* **88**, 133114 (2006)
12. H.L. Porter, A.L. Cai, J.F. Muth, J. Narayan, Enhanced photoconductivity of ZnO films Co-doped with nitrogen and tellurium. *Appl. Phys. Lett.* **86**, 211918 (2005)
13. S.J. Young, Y.H. Liu, Ultraviolet photodetectors with Ga-doped ZnO nanosheets structure. *Microelectron. Eng.* **148**, 14–16 (2015)
14. J. Lv, Y. Sun, L. Cao, M. Zhao, F. Shang, S. Mao, Y. Jiang, J. Xu, F. Wang, Z. Zhou, Y. Wei, G. He, M. Zhang, X. Song, Z. Sun, Effect of reaction temperature on surface morphology and photoelectric properties of ZnO grown by hydrothermal method in mixed solvent. *J. Mater. Sci. Mater. Electron.* **26**, 5518–5523 (2015)
15. J.J. Lai, Y.J. Lin, Y.H. Chen, H.C. Chang, C.J. Liu, Y.Y. Zou, Y.T. Shih, M.C. Wang, Effects of Na content on the luminescence behavior, conduction type, and crystal structure of Na-doped ZnO films. *J. Appl. Phys.* **110**, 013704 (2011)
16. J. Lue, J. Dai, J. Zhu, X. Song, Z. Sun, Effect of Na concentrations on microstructure and optical properties of ZnO films. *J. Wuhan Univ. Technol. Mater. Sci. Ed.* **26**, 23–27 (2011)
17. L.W. Wang, F. Wu, D.X. Tian, W.J. Li, L. Fang, C.Y. Kong, M. Zhou, Effects of Na content on structural and optical properties of Na-doped ZnO thin films prepared by sol–gel method. *J. Alloys Compd.* **623**, 367–373 (2015)
18. K.M. Lin, P. Tsai, Growth mechanism and characterization of ZnO: Al multi-layered thin films by sol-gel technique. *Thin Solid Films* **515**, 8601–8604 (2007)
19. T.P. Rao, M.C.S. Kumar, S.A. Angayarkanni, M. Ashok, Effect of stress on optical band gap of ZnO thin films with substrate temperature by spray pyrolysis. *J. Alloys Compd.* **485**, 413–417 (2009)
20. S.W. Xue, X.T. Zu, W.L. Zhou, H.X. Deng, X. Xiang, L. Zhang, H. Deng, Effects of post-thermal annealing on the optical constants of ZnO thin film. *J. Alloys Compd.* **448**, 21–26 (2008)
21. K. Siraj, K. Javaid, J.D. Pedarnig, M.A. Bodea, S. Naseem, Electron beam induced nanostructures and band gap tuning of ZnO thin films. *J. Alloys Compd.* **563**, 280–284 (2013)
22. V. Etacheri, R. Roshan, V. Kumar, Mg-doped ZnO nanoparticles for efficient sunlight-driven photocatalysis. *ACS Appl. Mater. Interfaces* **4**, 2717–2725 (2012)
23. S. Suwanboon, P. Amornpitoksuk, P. Bangrak, N. Muensit, Optical, photocatalytic and bactericidal properties of  $Zn_{1-x}La_xO$  and  $Zn_{1-x}Mg_xO$  nanostructures prepared by a sol–gel method. *Ceram. Int.* **39**, 5597–5608 (2013)

24. B. El Filali, T.V. Torchynska, A.I. Diaz Cano, Photoluminescence and Raman scattering study in ZnO: Cu nanocrystals. *J. Lumin.* **161**, 25–30 (2015)
25. D. Anbuselvan, S. Muthukumaran, Defect related microstructure, optical and photoluminescence behaviour of Ni, Cu co-doped ZnO nanoparticles by co-precipitation method. *Opt. Mater.* **42**, 124–131 (2015)
26. J.H. Yang, J.H. Zheng, H.J. Zhai, L.L. Yang, Y.J. Zhang, J.H. Lang, M. Gao, Growth mechanism and optical properties of ZnO nanotube by the hydrothermal method on Si substrates. *J. Alloys Compd.* **475**, 741–744 (2009)
27. J. Yang, J. Zheng, H. Zhai, X. Yang, L. Yang, Y. Liu, J. Lang, M. Gao, Oriented growth of ZnO nanostructures on different substrates via a hydrothermal method. *J. Alloys Compd.* **489**, 51–55 (2010)
28. M. Kashif, U. Hashim, M.E. Ali, S.M.U. Ali, M. Rusop, Z.H. Ibupoto, M. Willander, Effect of different seed solutions on the morphology and electrooptical properties of ZnO nanorods. *J. Nanomater.* **2012**, 452407 (2012)
29. K.K. Kim, H.S. Kim, D.K. Hwang, J.H. Lim, S.J. Park, Realization of p-type ZnO thin films via phosphorus doping and thermal activation of the dopant. *Appl. Phys. Lett.* **83**, 63–65 (2003)
30. J. Lv, P. Yan, M. Zhao, Y. Sun, F. Shang, G. He, M. Zhang, Z. Sun, Effect of ammonia on morphology, wettability and photoresponse of ZnO nanorods grown by hydrothermal method. *J. Alloys Compd.* **648**, 676–680 (2015)
31. X. Xu, C. Xu, J. Hu, High-performance deep ultraviolet photodetectors based on ZnO quantum dot assemblies. *J. Appl. Phys.* **116**, 103105 (2014)
32. C.F. Dee, S.K. Chong, S.A. Rahman, F.S. Omar, N.M. Huang, B.Y. Majlis, M.M. Salleh, Hierarchical Si/ZnO trunk-branch nanostructure for photocurrent enhancement. *Nanoscale Res. Lett.* **9**, 469 (2014)